Performance of Jason-2/GM altimeter in deriving marine gravity with the waveform derivative retracking method: a case study in the South China Sea

Zhen Li[1] · Xin Liu[1] · Jinyun Guo[1] · Chengcheng Zhu[1] · Jiajia Yuan[1] · Jinyao Gao[2] · Yonggang Gao[3] · Bing Ji[4]

Abstract

Deriving marine gravity is one of the important applications of satellite altimetry in earth science. The quality of marine gravity derived from each altimeter data always is limited by the range measurement on the certain ground track spacing. We assess the performance of Jason-2/geodetic-mission (GM) altimeter in deriving marine gravity by the improved range from waveform retracking. The singular value decomposition was applied to denoise waveforms, and the waveform derivative retracking was employed to improve the sea surface heights (SSHs). Finally, Jason-2/GM-derived gravity anomalies on $1' \times 1'$ grids were determined by the least-squares collocation method based on the resample 5 Hz SSHs around the South China Sea (SCS). Assessed by ship-borne data from different institutions, the accuracy of Jason-2/GM-derived gravity is consistent with that of the V27.1 and DTU13 models. Moreover, with the application of waveform derivative retracking, the accuracy of gravity anomalies has improved from 6.6 mGal before retracking to 5.5 mGal after retracking over the open ocean, and from 8.9 to 7.4 mGal over the coastal area. It is better than the results obtained by traditional retracking methods, including off-center of gravity (OCOG), 5-β, threshold, Ice-1, and maximum likelihood estimator-4 (MLE4). Furthermore, evaluated by V27.1 and DTU13, the result shows root mean square (RMS) difference of 2.0 mGal and 3.0 mGal, respectively. Therefore, the waveform derivative retracking is an effective method for altimeter data, and the accuracy of derived gravity is an improvement by retracked SSHs.

Keywords Marine gravity · Satellite altimetry · Waveform retracking · Waveform derivative · Jason-2/geodetic mission · Ship-borne gravimetry

Introduction

Satellite altimetry has wide applications in earth science, where it provides precise sea surface heights (SSHs) all over

✉ Xin Liu
xinliu1969@126.com

1   College of Geodesy and Geomatics, Shandong University of Science and Technology, Qingdao 266590, China

2   Second Institute of Oceanography of MNR, Hangzhou 310012, China

3   College of Environment and Resources, Fuzhou University, Fuzhou 350108, China

4   Department of Navigation Engineering, Naval University of Engineering, Wuhan 430033, China

the world (Shum et al. 1995; Guo et al. 2016; Stammer and Cazenave 2017; Yuan et al. 2020a). The SSHs are used to derive global and regional marine gravity (Hwang et al. 2006; Sandwell et al. 2013; Khaki et al. 2015). Marine gravity derived from satellite altimeter data can reveal more localized information than that provided by satellite gravity missions (Sandwell et al. 2014; Zhu et al. 2020). Moreover, it takes less time and gets more repeatable data in a significant range with respect to ship-borne or airborne gravity data (Zhang et al. 2018). The quality of SSHs is closely related to the altimeter echo waveforms. As the waveform over a complex area is susceptible to the effects of the land, island, and sea surface conditions, the retrieving SSH accuracy is limited (Tseng et al. 2013; Arabsahebi et al. 2018).

In order to improve the quality of SSH, several retrackers have been developed. The waveform retracking methods are mainly divided into two categories based on either full-waveform or sub-waveform (Anzenhofer et al. 1999;

Gommenginger et al. 2011), including the function fitting and the empirical statistical methods. The sub-waveform is defined as the partial waveform. It is beneficial to obtain reliable SSH by sub-waveform retracking, but the identification of sub-waveform is difficult (Idris and Deng 2012; Passaro et al. 2014). The function fitting method is used to retrieve geophysical parameters on the basis of the function model. It is related to the physical properties of ocean reflecting surface, such as the maximum likelihood estimator-4 (MLE4) method (Amarouche et al. 2004). The MLE4 method has been used as the standard ocean retracker for most altimeter data (Dumont et al. 2011). This kind of method has a clear physical explanation and higher calculation accuracy (Martin et al. 1983; Peng and Deng 2017). The other empirical method is developed on the pre-defined statistical equations, such as off-center of gravity (OCOG) (Wingham et al. 1986) and threshold retrackers (Davis 1997). It has a high adaptability and provides a robust estimate of range for complex waveform shapes (Huang et al. 2017; Roscher et al. 2017). However, the performance of each single retracker has certain limitations, for example, the estimated range of function fitting method is affected by the waveform shapes and the physical explanation of empirical method is unclear (Gommenginger et al. 2011; Arabsahebi et al. 2018). Therefore, considering the complexity of waveform over a region, the single kind of method is not always optimal retracker (Idris 2019; Yuan et al. 2020b).

Waveform retracking plays an important role in improving the accuracy of marine gravity derived from satellite altimeter data. On the basis of sub-waveform, the retracked SSHs are obtained by the threshold or 5-β method (Martin et al. 1983), improving the accuracy of derived gravity anomalies in the coastal area (Hwang et al. 2006; Guo et al. 2010; Yang et al. 2012). To improve the regional gravity anomalies, the extrema retracking method (Khaki et al. 2015) based on edge detection and extracting extremum points is applied to waveform over a region. Moreover, in order to optimize the global marine gravity model derived by satellite altimetry, a two-step waveform retracking is employed (Andersen et al. 2010; Garcia et al. 2014). In the first retracking step, all three parameters (amplitude, range, and significant wave height) are estimated and the significant wave height (SWH) is smoothed along ground track. In the second step, the SWH is fixed to a known value and re-estimated the range correction and amplitude. The two-step retracking method improves the range precision by a factor of 1.5 for sea surface slopes, but it does not result in an improvement in the precision of absolute SSHs (Hwang and Chang 2014; Zhang et al. 2017).

With the development of satellite altimetry technology, the method of derivation of gravity anomalies by satellite altimetry is gradually mature (Rap, 1979; Andersen et al. 2010; Sandwell et al. 2013). The least-squares collocation (LSC) method is used to determine gravity anomalies based on the remove-restore procedure (Hwang 1989; Andersen and Knudsen 1998). The advantage of LSC is that the process is stable and the result is smooth (Shih et al. 2015). Moreover, the LSC is able to combine multiple types of data for gravity anomaly derivation (McCubbine et al. 2017). Based on LSC, the gravity anomalies are derived from different satellite altimeter data and their accuracy is reliable (Hwang et al. 2006; Zhu et al. 2019).

Jason-2 is the follow-on to TOPEX/Poseidon and Jason-1, whose main features have been inherited (Dumont et al. 2011). The Jason-2 altimeter has the same characteristics with Jason-1, but with a lower instrument noise. It is usually used as a reference to the accuracy evaluation for other altimeters (Bao et al. 2015; Prandi et al. 2015). The geodetic mission (GM) of Jason-2 is carried out from July 2017 after the exact repeat mission. It has collected a large amount of high-resolution GM altimeter data. The GM data provides denser spatial coverage in the derivation of marine gravity, such as Geosat/GM, Jason-1/GM, and HY-2A/GM (Garcia et al. 2014; Zhu et al. 2019). Therefore, we assess the performance of Jason-2 altimeter in deriving marine gravity by retracked SSHs of GM.

The paper is organized as follows: the data used in this study are explained in the "Data" section. In order to improve the quality of Jason-2/GM altimeter data, the waveform derivative retracking method is provided in the "Satellite altimetry retracking" section. The discussion of waveform SVD denoise and the result of derived gravity anomalies by retracked SSHs on 1′ × 1′ grid around the South China Sea (105°–125° E, 0°–30° N) is shown in the "Results and discussions" section. The performance of Jason-2/GM-derived gravity anomalies with waveform derivative retracking method is analyzed in the "Comparison and analysis" section. Finally, the study is concluded in the "Conclusion" section.

Data

Altimeter data

The latest version D of Sensor Geophysical Data Records (SGDR) from Jason-2/GM is released by AVISO (Archiving, Validation, and Interpretation of Satellite Oceanographic, http://www.aviso.altimetry.fr/). The SGDR products include the waveform data of 20 Hz and current state-of-the-art geophysical corrections which are necessary to compute SSH. The Jason-2/GM altimeter data from July 2017 to July 2018 was used, corresponding to the data files from cycles 500 to 537. The Jason-2/GM ground tracks within the South China Sea and its adjacent areas are shown in Fig. 1, and the data in cycles 506 and 507 are missing. In this complex region, the waveform is susceptible to contamination from the land, island, and sea surface conditions. The
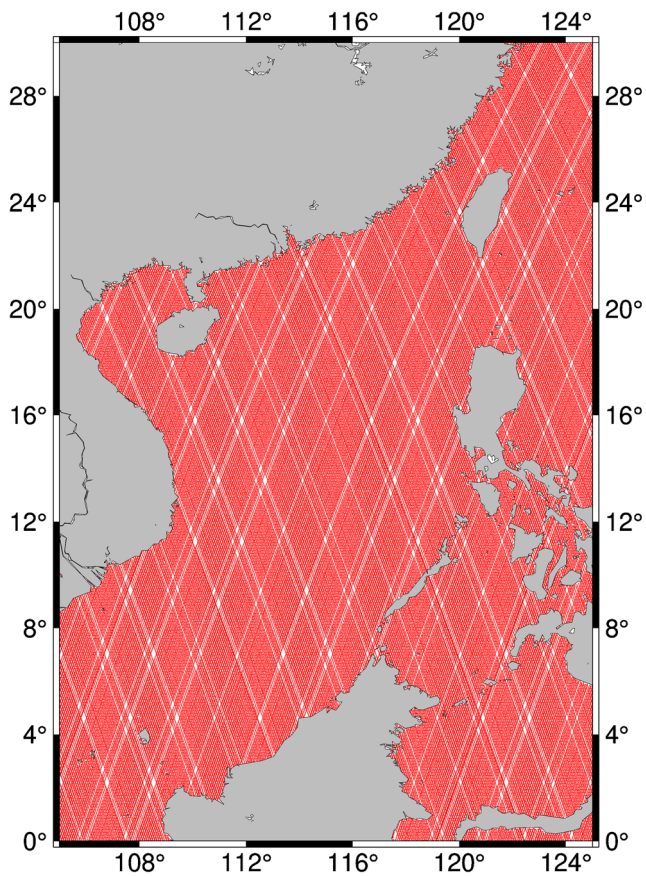
Fig. 1 Jason-2/GM ground tracks around the South China Sea

waveforms of a ground track (cycle520 pass177) are shown in Fig. 2. To improve the quality of SSH, it is necessary to retrack waveform over the SCS.

Ship-borne gravity data

To assess the precision of Jason-2/GM-derived gravity anomalies with waveform derivative retracking method, a comparison is done with ship-borne gravity data provided by the US National Center for Environmental Information (NCEI) and the Second Institute of Oceanography (SIO), Ministry of
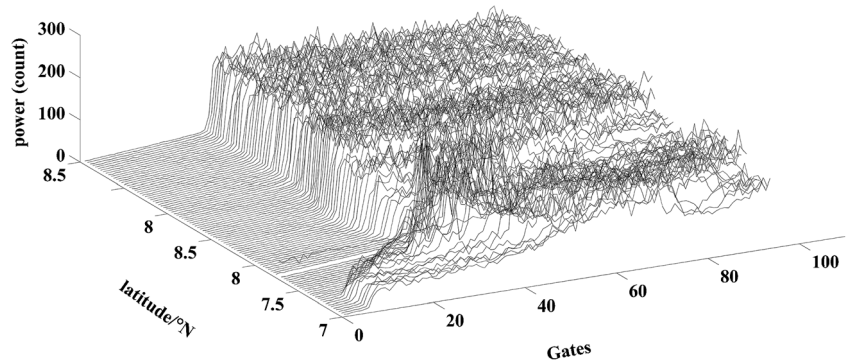
Natural Resources of P. R. China. The NCEI ship-borne data includes 461652 points measured by 85 cruises from 1967 to 2010 (https://maps.ngdc.noaa.gov/viewers/geophysics/). Most of the NCEI ship-borne data are taken before the 1990s; the accuracy is affected by navigation accuracy. The SIO ship-borne gravity is measured from 1999 to 2010, with better data quality. It includes 13288 points measured by 17 cruises. Since the NCEI, ship-borne gravity is obtained from different organizations, which cause that the ship-borne data contain systematic errors, such as the drift error of gravimeter and the error between different reference gravity fields (Wessel and Watts 1988).

Marine gravity models V27.1 and DTU13

Due to the limitations of ship-borne gravity data, the Jason-2/ GM-derived gravity anomalies with waveform derivative retracking method are also compared with the high-accuracy global marine gravity models V27.1 (Sandwell et al. 2013) and DTU13 (Andersen et al. 2014). The V27.1 is released on March 2019 by Scripps Institution of Oceanography (https://topex.ucsd.edu/). The altimeter data used in the V27. 1 is from CryoSat-2, Jason-1, Geosat, and ERS-1 (Garcia et al. 2014). The model has a high resolution of $1' \times 1'$ on the global, including 1431288 grid points around the SCS.

The DTU13 is released by the Technical University of Denmark. It is derived not only by the retracked SSHs from CryoSat-2, Jason-1, and so on but also by the combination of airborne gravity data and laser altimetry from ICESat (Andersen et al. 2010). The DTU13 model also has a high resolution of $1' \times 1'$ on the global, including 1382108 grid points around the SCS.

EGM2008

Earth gravitational field model (EGM2008) is a high-precision spherical harmonic function model of the global gravitational field model (http://earth-info.nga.mil/GandG/ wgs84/gravitymod/egm2008). EGM2008 up to degree and

Fig. 2 Waveform data (cycle520 pass177)

order 2160 is used to compute a series of products, such as vertical deflection, gravity anomalies, and geoid heights. (Pavlis et al. 2012; Wang et al. 2018). In this study, it is selected as the reference gravitational field.

Satellite altimetry retracking

Waveform SVD denoising

The echo waveform of satellite radar altimeter is a set of discrete gate power. Each gate power includes the echo signal from ocean reflection surface and speckle noise. However, the existence of noise influences the result of waveform retracking (Halimi et al. 2017; Xu et al. 2018). For this reason, the singular value decomposition (SVD) is applied to denoise waveforms (Ollivier 2006; Thibaut et al. 2009). The idea of SVD denoise is to eliminate the minor singular value of waveform components, since those components are considered to be caused by noises rather than ocean echo signals. The procedure is as follows:

(1) Arrange L ($>N$, the number of the waveform gates) consecutive waveforms form a waveform matrix: $\boldsymbol{W}(N \times L)$;
(2) SVD of waveform matrix $\boldsymbol{W}(N \times L)$:

$$\boldsymbol{W} = \boldsymbol{U} \times \boldsymbol{S} \times \boldsymbol{V}' \tag{1}$$

where U and V are both orthogonal matrixes, and S is a diagonal matrix, whose diagonal elements are sorted from large to small:

$$S = diag(s_1, \ s_2, \ s_3 \ldots s_N) \tag{2}$$

(3) Select the percentage T of waveform singular according to the following conditions:

$$\sum_{i=1}^{k-1} s_i < T * \sum_{i=1}^{N} s_i, \ \sum_{i=1}^{k} s_i \geq T * \sum_{i=1}^{N} s_i \tag{3}$$

(4) Reconstruct the waveform matrix W_{SVD}:

$$\boldsymbol{W_{SVD}} = \boldsymbol{U} \times \boldsymbol{S_k} \times \boldsymbol{V}' \tag{4}$$

The percentage T of waveform singular affects the quality of denoising waveform. If the value is large, the noise of waveform cannot be eliminated. If it is small, the effective signal can be removed. The different percentage is discussed in the "Results and discussions" section.

Waveform derivative retracking method

On the basis of analysis radar altimeter echo principle and the waveform model, Brown (1977) demonstrated the echo received from ocean target has a typical rising part (leading edge). The leading edge of the waveform model is an odd function with respect to the midpoint of the leading edge (Vignudelli et al. 2019; Gommenginger et al. 2011). Therefore, the leading edge midpoint can be determined by the maximum value of the leading edge slope, i.e., the zero of the second waveform derivative function. The theoretical waveform model is the Brown model (Brown 1977), which describes the average return power as a function of delay time, expressed as:

$$W(t) = A_p \exp(-v)(1 + \mathrm{erf}(u)) + T_n \tag{5}$$

where

$$v = a\left[(t-t_0) - \frac{a}{2}\sigma_c^2\right] \qquad u = \frac{(t-t_0) - a \times \sigma_c^2}{\sqrt{2}\sigma_c}$$

$$a = a - \frac{\beta^2}{4} \qquad a = \frac{\ln 4}{\sin^2\left(\theta/_2\right)} \times \frac{c}{h} \times \frac{1}{1 + h/_R} \times \cos(2\xi)$$

$$A_p = \frac{A_0}{2}\exp\left(-\frac{4}{\gamma}\sin^2\xi\right) \quad \beta = \frac{\ln 4}{\sin^2\left(\theta/_2\right)} \times \sqrt{\frac{c}{h} \times \frac{1}{1 + h/_R}} \times \sin(2\xi)$$

where h is the satellite altitude, R is the radius of the Earth, c is the speed of light in vacuum, A_0 is the amplitude of waveform, θ is the antenna beam width, ξ is the antenna off-nadir mispointing angle, t_0 is the epoch with respect to the nominal tracking reference point, σ_c is the rise time of the leading edge, γ is the parameter related to the beam width, T_n is the thermal noise level, and $\mathrm{erf}(x)$ is the error function.

Based on Eq. (5), the functions of the first and second waveform derivative are given as:

$$W'(t) = A_p \times \exp(-v)\left[-a \times (1 + \mathrm{erf}(u)) + \frac{\sqrt{2}}{\sqrt{\pi}\sigma_c} \times \exp(-u^2)\right] \tag{6}$$

$$W^{\}}(t) = A_p \times \exp(-v) \times \left[a^2 \times (1 + \mathrm{erf}(u)) - \frac{2\sqrt{2a}}{\sqrt{\pi}\sigma_c} \times \exp(-u^2) - \frac{2u}{\sqrt{\pi}\sigma_c^2} \times \exp(-u^2)\right] \tag{7}$$

At the position of maximum slope of leading edge, the leading edge midpoint is determined by the zero of the second waveform derivative function ($W'' = 0$). It is expressed as

$$t_m = t_0 - a\sigma_c^2 \tag{8}$$

where the t_0 and σ_c are the unknown parameters.

In order to more accurately determine the leading edge midpoint on the measured waveform, combining the advantages of the empirical statistical retracker (similar to threshold method), the leading edge midpoint is redetermined. The leading edge midpoint power value is obtained by Eq. (5), which is linearly interpolated to the adjacent power value of the leading edge of measured waveform to redetermine the midpoint, i.e.,

$$t_{rm} = \left(\widehat{n} - 1\right) + \frac{W_m - W_{\widehat{n}-1}}{W_{\widehat{n}} - W_{\widehat{n}-1}} \tag{9}$$

where t_{rm} is the re-determined leading edge midpoint, W_m is the estimated midpoint power by Eq. (5), $\widehat{n}$ is the first gate position beyond the estimated midpoint power, and $W_{\widehat{n}}$ and $W_{\widehat{n}-1}$ are the measured waveform power respectively.

Determination of midpoint

Based on the waveform model, there are five unknown parameters in Eq. (5): A_0, t_0, σ_c, T_n, ξ. Generally, the thermal noise T_n is less than 3% of waveform amplitude; it can be estimated by the first few waveform gates (Gommenginger et al. 2011). The off-nadir mispointing angle provided by the Jason-2 SGDR products can be used due to its very small value (usually less than 0.3°) and improved accuracy (Amarouche et al. 2004). Thus, in order to calculate the leading edge midpoint, we estimate three unknown parameters, i.e., A_0, t_0, and σ_c.

Three unknown parameters are estimated based on the measured waveform. They are solved using the least-squares estimator (Gommenginger et al. 2011). The leading edge midpoint is determined by the estimated parameters t_0 and σ_c according to Eqs. (8) and (9). It is called the first waveform derivative retracker (FWDR) in this paper.

Moreover, to improve the accuracy of three unknown parameters to be estimated, they are re-estimated based on the first-order difference quotient of waveform. Because the noise of waveform cannot be completely eliminated by SVD denoise, it can be further reduced by the first-order difference quotient of waveform, such as thermal noise. The first-order difference quotient of waveform, $W'\left(t_{k+^1/_2}\right)$, can be computed as,

$$W'\left(t_{k+^1/_2}\right) = \frac{W(t_{k+1}) - W(t_k)}{\Delta t} \tag{10}$$

where $W(t_{k+1})$ and $W(t_k)$ are the echo powers corresponding to the gates $k+1$ and k respectively, Δt is the sampling interval. Equation (10) is indicated that the $W'\left(t_{k+^1/_2}\right)$ is correlated between different gates.

Three unknown parameters (A_0, t_0, σ_c) are estimated using the weighted least-squares estimator. The weight $\boldsymbol{P}$ is determined based on the covariance propagation law as,

$$\boldsymbol{P} = \begin{bmatrix} 2 & -1 & 0 & \ldots & 0 \\ -1 & 2 & -1 & \ldots & 0 \\ 0 & -1 & 2 & \ldots & 0 \\ \ldots & \ldots & \ldots & \ldots & -1 \\ 0 & \ldots & 0 & -1 & 2 \end{bmatrix}_{(n-1)\times(n-1)}^{-1} \tag{11}$$

The leading edge midpoint is determined by the re-estimated parameters t_0 and σ_c. It is called the second waveform derivative retracker (SWDR) in this paper.

Retracked SSH

The SSH is defined as,

$$SSH = H_{alt} - \left(Tracker + Corr_{doppler} + Corr_{model} + Corr_{system\_bias} + Corr_{Dry} + Corr_{Wet} + Corr_{Iono} + Corr_{Ib} + Corr_{hf} + H_{ocean} + H_{solid} + H_{pole} + R_{retracking}\right) \tag{12}$$

where H_{alt} is the Jason-2 satellite altitude, $Tracker$ is the range between satellite and reflective surface (partial instrumental corrections included, i.e., distance antenna-COG, USO drift correction, internal path correction), $Corr_{doppler}$ is the Doppler correction, $Corr_{model}$ is the modeled instrumental correction, $Corr_{system\_bias}$ is the system bias of instrument, $Corr_{Dry}$ is the dry tropospheric correction, $Corr_{Wet}$ is the wet tropospheric correction, and $Corr_{Iono}$ is the ionospheric delay correction. The numerical prediction models from the European Centre for Medium-Range Weather Forecasts (ECMWF) are applied for $Corr_{Wet}$ and $Corr_{Iono}$. $Corr_{Ib}$ (inverted barometer correction) and $Corr_{hf}$ (high-frequency atmospheric pressure loading correction) are the dynamic atmospheric corrections, H_{ocean} is the geocentric ocean tide height correction, H_{solid} is the solid earth tide height correction, and H_{pole} is the pole tide height correction. These above corrections are available in the SGDRs, and the outliers of geophysical correction are eliminated by the data editing criteria (Dumont et al. 2011). $R_{retracking}$ is the range correction of waveform retracking.

The range correction of waveform derivative retracking is given as,

$$R_{retracking} = (t_{rm} - \tau) \times \frac{c \times \Delta G_a}{2} \tag{13}$$

where t_{rm} is the leading edge midpoint, τ is the nominal tracking gate ($\tau = 32$ gate of Jason-2 altimeter waveform), and ΔG_a is the sampling interval of a gate (1 gate = 3.125 ns of Jason-2 altimeter).

Results and discussions

Analysis of SVD denoise

In order to analyze the performance of waveform SVD denoise, we tested three typical percentage T of SVD: 90%, 80%, and 70%. The standard deviation (STD) of 20 Hz retracked SSHs is computed, and the total number is 187347. The median of standard deviation is listed in Table 1. In the procedure of calculation, because the geoid gradients with rapidly changing can increase the STD (Gommenginger et al. 2011), the geoid height of 1 Hz derived by EGM2008 is selected as the mean value instead of the simple average value.

Table 1 represents that the STDs of 20 Hz retracked SSHs with waveform SVD denoise are less than of without SVD denoise. It is indicated that the waveform SVD can reduce the effect of waveform noise, and improve the quality of retracked SSHs. From empirical method, such as OCOG and threshold 50%, the improvement of STD is slight. The reason is that the range correction of empirical method mainly depends on the pre-defined equations. From the function fitting method, such as 5-β, FWDR, and SWDR, the improvement of STD is more obvious. This is because the smooth waveform is beneficial to obtain accurate parameter estimation for the function fitting method. From Table 1, it is notable that the STD of 80% SVD is less than of other SVD denoise. Consequently, the 80% SVD of waveform denoise is selected in this paper.

The 1 Hz data correspond to the distance of ground along-track about 6 km (Dumont et al. 2011). The high rate data can improve the resolution of along-track SSHs comparison with 1 Hz data (Zhang et al. 2017). The number of 5 Hz SSHs meets the 1′ × 1′ grids data requirement of along-track. Therefore, the retracked 20 Hz SSHs are resampled at 5 Hz, and the Gauss filter with a window length of 20 km is used to reducing the noise of 20 Hz SSH.

Table 1 The median of standard deviation (unit: cm)

Percentage of SVD	No SVD	90% SVD	80% SVD	70% SVD
OCOG	15.7	15.4	15.3	15.3
5-β	11.9	11.3	11.0	11.2
Threshold 50%	9.6	9.7	9.5	9.4
FWDR	9.4	9.0	8.7	8.9
SWDR	9.1	8.8	8.5	8.7

Altimeter-derived gravity anomalies based on LSC

The least-squares collocation (LSC) method is used to deriving gravity anomalies based on remove-restore technique (Yang et al. 2012; Zhu et al. 2019). The residual geoid gradients are determined by the geoid gradients computed by the retracked SSH removing the reference geoid gradients of EGM20008. Then, the residual gravity anomalies are determined by the residual geoid gradient, and the final gravity anomalies are obtained by restoring reference gravity anomalies of EGM2008. Based on the LSC, the residual gravity anomalies are computed by Hwang and Parsons (1995):

$$\Delta \boldsymbol{g}_{res} = \boldsymbol{C}_{\Delta ge}(\boldsymbol{C}_{ee} + \boldsymbol{C}_{nn})^{-1}\boldsymbol{e}_{res} \qquad (14)$$

where $\Delta \boldsymbol{g}_{res}$ is the vectors of residual gravity anomalies, $\boldsymbol{e}_{res}$ is the residual geoid gradients, $\boldsymbol{C}_{\Delta ge}$ is the covariance matrices for gravity anomaly-residual geoid gradients, $\boldsymbol{C}_{ee}$ is the covariance matrices for gravity anomaly-gravity anomaly, and $\boldsymbol{C}_{nn}$ is the diagonal matrix holding the noise of residual geoid gradient.

The $\boldsymbol{C}_{\Delta ge}$ and $\boldsymbol{C}_{ee}$ can be derived by the parameters of gravity field, including the covariance of gravity anomaly-gravity anomaly $\boldsymbol{C}_{\Delta g\Delta g}$, the covariance of longitudinal gradient-gravity anomaly $\boldsymbol{C}_{l\Delta g}$, the covariance of longitudinal-longitudinal gradient $\boldsymbol{C}_u$, and the transverse-transverse gradient $\boldsymbol{C}_{mm}$ (Hwang 1989). Furthermore, all parameters of the gravity field can be expressed as the functional of anomalous gravity potentials. The covariance of anomalous gravity potentials is homogeneous and isotropic, so parameters of gravity field are only related to the distance between two points on the reference ellipsoid. As shown in Fig. 3, when the spherical distance is greater than 0.5°, the covariance of gravity field related parameters are close to 0, indicating that the gravity anomaly and geoid gradient have little correlation.

Accordingly, the gravity anomalies are calculated with different spherical distances in the range of 0.1° to 0.5°. The results are list in Table 2. The result of FWDR and SWDR is the root mean square (RMS) difference between Jason-2/GM-derived gravity anomalies with the waveform derivative retracking method and the NCEI ship-borne gravity anomalies. In the span of 0.1° to 0.4°, while the spherical distance increases, the RMS difference between Jason-2/GM-derived and NCEI ship-borne gravity anomalies gradually decreases, but the RMS is increased when the distance is 0.5°. The main reason is that the little correlation between the gravity anomaly and geoid gradient affects the accuracy of satellite altimeter-derived gravity anomalies. Therefore, the altimeter-derived gravity anomalies on the spherical distance of 0.4° are selected in this paper.

Fig. 3 Covariance of gravity field parameters, **a** is the covariance of gravity anomaly-gravity anomaly $C_{\Delta g \Delta g}$, **b** is the covariance of longitudinal gradient-gravity anomaly $C_{l\Delta g}$, **c** is the covariance of longitudinal-longitudinal gradient C_{ll} and the transver-transverse gradient C_{mm}.
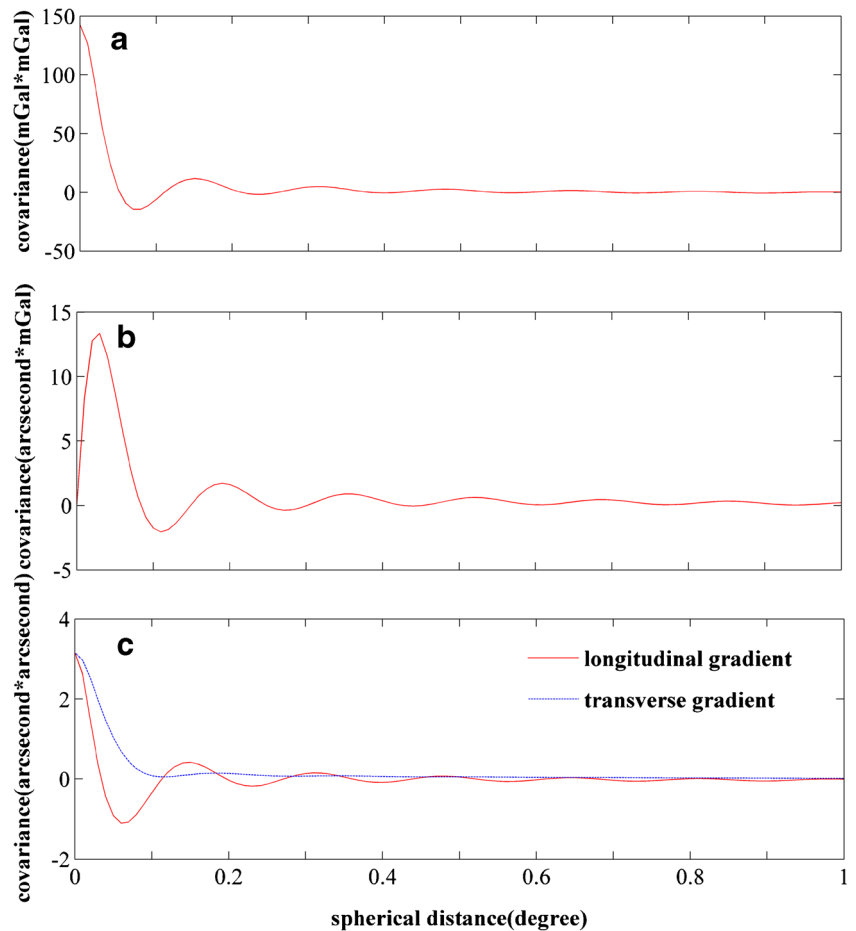
The Jason-2/GM altimeter-derived gravity anomalies with SWDR on $1' \times 1'$ grid around the SCS are shown in Fig. 4.

Comparison and analysis

Comparison with ship-borne data

A direct assessment of the Jason-2/GM-derived gravity anomalies with waveform derivative retracking is carried out: comparison with NCEI and SIO ship-borne gravity anomalies. Before comparison, the systematic errors of ship-borne gravity caused by different organizations are removed and the outliers are deleted using the three-sigma criterion (Hwang and Parsons 1995; Zhu et al. 2019). The remaining NCEI and SIO ship-borne gravity anomalies are 451453 points and 13288 points, respectively. The differences between the Jason-2/GM-derived gravity anomalies with SWDR and ship-borne gravity anomalies are shown in Fig. 5. The statistical results are shown in Table 3.

The NCEI ship-borne data has a large number of measurements and is distributed throughout the region (Fig. 5a). The RMS difference between Jason-2/GM-derived gravity anomalies with waveform derivative retracking method (FWDR and SWDR) and NCEI ship-borne gravity anomalies both is 5.8 mGal. To assess the accuracy of the results, the RMS difference between the high-accuracy gravity field models (V27.1 and DTU13) and the ship-borne data are also computed. The RMS difference between the V27.1-derived and the ship-borne gravity anomalies is 5.1 mGal, and is 5.4 mGal when replacing the V27.1 from the DTU13. The accuracy of Jason-2/GM-derived gravity anomalies with waveform derivative retracking is consistent with the DTU13 and V27.1 over the region.

Additionally, the gravity results are compared with the SIO ship-borne gravity with better data quality, which is mainly

Table 2 Statistical results of different spherical distances (unit: mGal)

Spherical distance/°	0.1	0.2	0.3	0.4	0.5
FWDR	5.87	5.86	5.85	5.84	5.85
SWDR	5.87	5.86	5.84	5.83	5.85
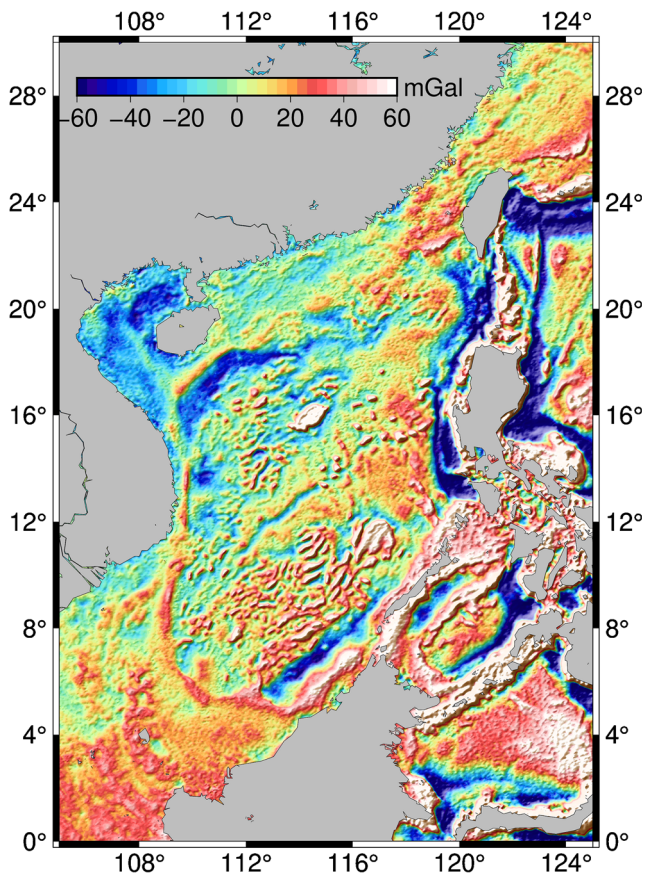
Fig. 4 Jason-2/GM-derived gravity anomalies with SWDR around the SCS

distributed in the SCS. The RMS difference between Jason-2/GM-derived gravity anomalies with waveform derivative retracking method (FWDR and SWDR) and SIO ship-borne gravity anomalies both is 2.9 mGal. The RMS difference between the V27.1-derived and the SIO ship-borne gravity anomalies is 2.8 mGal, and is 2.5 mGal when replacing the V27.1 from the DTU13. Thus, it is indicated that the Jason-2/GM-derived gravity anomalies with waveform derivative retracking are reliable.

Comparison with different waveform retracking methods

To assess the improvement of Jason-2/GM-derived gravity with waveform deriving retracking method, the altimeter-derived gravity by raw and retracked SSHs from common waveform retracking methods is also compared with the NECI ship-borne data. The common methods include off-center of gravity (OCOG), 5-β, threshold, Ice-1 (Wingham et al. 1986), and maximum likelihood estimator-4 (MLE4). For threshold method, there is no clear criterion for the selection of threshold

level. Here, the threshold level of 50% is selected for retracking waveforms over the region (Guo et al. 2006). The retracked SSHs of OCOG, 5-β, threshold, FWDR, and SWDR are from the waveform of SVD (80%) denoise. The Ice-1 method is similar to the threshold, and with threshold level of 30%. The retracked SSHs of Ice-1 and MLE4 are the standard products of SGDR. We compute the statistical results for ship-borne data where water depths are larger than 500 m and smaller than 500 m, on the basis of values interpolated from global topographic model ETOPO1.

The statistics of differences for NCEI ship-borne gravity anomalies over the open ocean (water depths larger than 500 m) are shown in Table 4. The raw represents the result of altimeter-derived gravity anomalies by unretracked SSHs. Table 4 is evident that the accuracy of altimeter-derived gravity anomalies is improved by retracked SSHs. The RMSs of difference obtained by FWDR and SWDR both are 5.5 mGal. They are smaller than that of obtained by OCOG, 5-β, Ice-1, and threshold method. In addition, the maximum and minimum of difference obtained by FWDR and SWDR are better than that of obtained by MLE4 method, while they have the same RMS with MLE4. Considering the RMS of difference obtained by the raw data of 6.6 mGal, the accuracy of Jason-2/GM-derived gravity anomalies with waveform derivative retracking method has been improved about 1.1 mGal over the open ocean.

The statistics of differences for NCEI ship-borne gravity anomalies over the coastal area (water depths smaller than 500 m) are shown in Table 5. The RMS of difference obtained by raw is 8.9 mGal, and the RMSs of difference obtained by FWDR and SWDR both are 7.4 mGal. It is indicated that the accuracy of Jason-2/GM-derived gravity anomalies with waveform derivative retracking method has been improved about 1.5 mGal over the coastal area. The improvement of RMS over the coastal area is better than that of over the open ocean. The main reason is that the waveforms over the coastal area are more susceptible to contamination. The RMSs of difference obtained by waveform derivative retracking method (FWDR and SWDR) are also smaller than that of obtained by OCOG, 5-β, Ice-1, MLE4, and threshold method. It is shown that the waveform derivative retracking method can combine the advantages of function fitting and empirical statistical methods, and get more reliable SSHs than common methods. Moreover, the maximum and minimum of difference obtained by SWDR are better than that of obtained by FWDR method, when the RMS difference is same.

Therefore, through comparison with the derived gravity anomalies by raw and retracked SSHs, it seems that the application of waveform retracking is highly beneficial for the
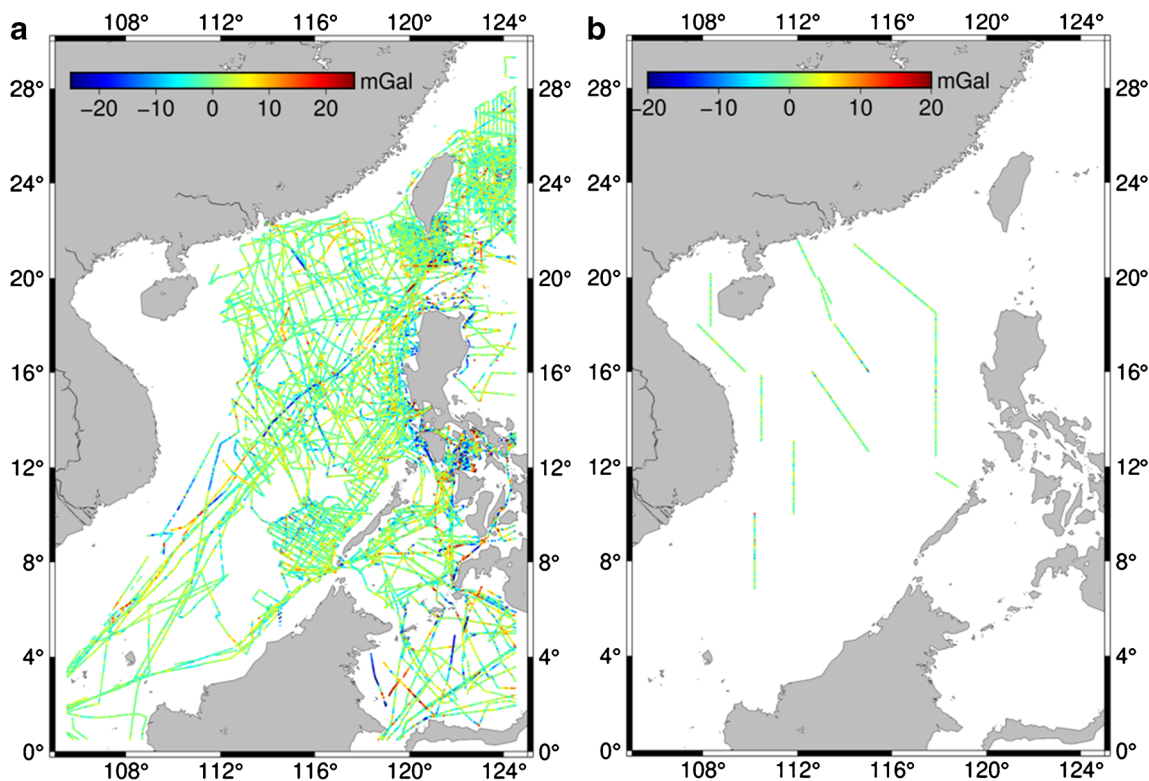
Fig. 5 Gravity difference. **a** is the difference between Jason-2/GM-derived gravity anomalies with SWDR and NCEI ship-borne gravity anomalies, **b** is the difference between Jason-2/GM-derived gravity anomalies with SWDR and SIO ship-borne gravity anomalies

derivation of gravity anomalies. The improvement of accuracy of Jason-2/GM-derived gravity anomalies with waveform derivative retracking method is better than that of traditional retrackers.

Comparison with the global marine gravity model

The Jason-2/GM-derived gravity anomalies with waveform derivative retracking method are also compared with the global marine gravity model V27.1 and DTU13. The results are interpolated to the grid points of model V27.1 and DTU13,

respectively. The grid points on land are eliminated by using GMT.

The differences between the Jason-2/GM-derived with SWDR and gravity model are shown in Fig. 6. The distance of the grid points to the coastline is computed (Wessel et al. 2013). The grid points are excluded in the different range of 0 to 50 km (interval: 10 km) away from coastline, respectively; the statistical results in the different distance are shown in Table 6. The Jason-2/GM_A-V27.1 represents the difference between Jason-2/GM-derived with SWDR and V27.1 model,

Table 3 Statistics of the difference between Jason-2/GM-derived and ship-borne gravity anomalies (unit: mGal)

	Ship-borne data (number)	Max	Min	Mean	STD	RMS
FWDR	NCEI (451453)	43.2	− 43.5	− 0.1	5.8	5.8
SWDR		42.2	− 42.6	− 0.1	5.8	5.8
V27.1		54.9	− 50.2	0.0	5.1	5.1
DTU13		47.0	− 42.3	− 0.1	5.4	5.4
FWDR	SIO (13288)	16.8	− 14.0	0.0	2.9	2.9
SWDR		15.5	− 13.2	0.0	2.9	2.9
V27.1		16.1	− 17.6	0.0	2.8	2.8
DTU13		17.5	− 12.6	0.1	2.5	2.5

Table 4 Statistics of the difference obtained by different retrackers over the open ocean (unit: mGal)

Retracker	Max	Min	Mean	STD	RMS
Raw	44.9	− 45.8	− 0.2	6.6	6.6
OCOG	43.9	− 44.9	− 0.2	6.1	6.1
5-β	45.1	− 44.0	− 0.2	5.7	5.7
Ice-1	43.1	− 43.7	− 0.2	5.7	5.7
Threshold	43.8	− 44.1	− 0.2	5.6	5.6
MLE4	43.9	− 43.8	− 0.2	5.5	5.5
FWDR	42.4	− 43.5	− 0.2	5.5	5.5
SWDR	42.1	− 42.6	− 0.2	5.5	5.5

Table 5 Statistics of the difference obtained by different retrackers over the coastal area (unit: mGal)

Retracker	Max	Min	Mean	STD	RMS
Raw	45.2	− 40.1	0.9	8.8	8.9
OCOG	42.3	− 39.7	0.9	7.8	7.9
5-β	41.5	− 39.3	0.9	7.6	7.7
Ice-1	42.7	− 37.7	0.8	7.5	7.6
MLE4	42.5	− 38.8	0.9	7.5	7.6
Threshold	43.6	− 37.1	0.9	7.4	7.5
FWDR	43.2	− 37.4	0.9	7.3	7.4
SWDR	42.2	− 37.2	0.9	7.3	7.4

and the Jason-2/GM_A-DTU13 represents the difference between Jason-2/GM-derived with SWDR and DTU13 model.

As can be seen from Table 6, in the range of 0 to 20 km, the RMSs of Jason-2/GM_A-V27.1 and Jason-2/GM_A-DTU13 are decreasing rapidly with the increase of distance from the coastline. In the range of 20 to 50 km, the RMSs have a small value of about 3.0 mGal and 2.0 mGal, respectively. This is indicated that the Jason-2/GM-derived gravity anomalies are consistent with V27.1 and DTU13 model from the 20 km away from coastline. Therefore, the accuracy of Jason-2/GM-derived gravity anomalies with waveform derivative retracking method is further verified.

The RMS difference over the coastal areas (about 20 km away from coastline) is larger than the RMS over the open ocean. It can be considered that the retracked SSHs in the last 20 km still contains some errors, such as lower accuracy tide model and sea station bias corrections.

Conclusion

Jason-2/GM altimeter has collected a large amount of high-resolution data. The accuracy of range measurement is reduced due to the contaminated waveform. To improve the quality of SSHs, the SVD is applied to denoise waveforms, and the waveform derivative retracking is employed to correct range. Finally, the Jason-2/GM altimeter-derived gravity anomalies by retracked SSHs on grid $1' \times 1'$ are determined by LSC around SCS.

The accuracy of Jason-2/GM-derived marine gravity with waveform derivative retracking method is evaluated by comparison with ship-borne data provided by NCEI and SIO, marine gravity derived from different waveform retracking methods, and global marine gravity V27.1 and DTU13. The RMS difference between Jason-2/GM-derived gravity anomalies with waveform derivative retracking method and NCEI ship-borne gravity anomalies is 5.8 mGal, and is 2.9 mGal when
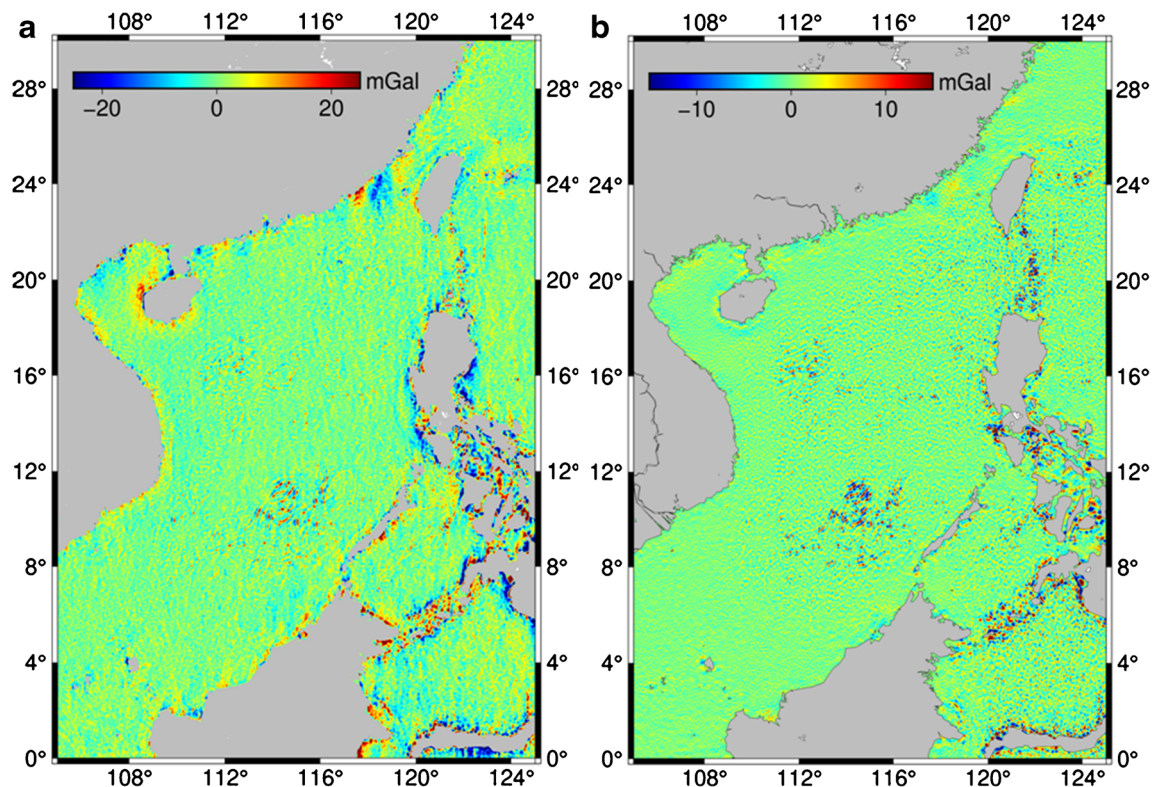
Fig. 6 Marine gravity differences. **a** is the difference between Jason-2/GM-derived and v27.1, **b** is the difference between Jason-2/GM-derived and DTU13

Table 6 The statistical results in different areas (unit: mGal)

Distance away from coastline	Jason-2/GM_A-V27.1			Jason-2/GM_A-DTU13		
	Number	Mean	RMS	Number	Mean	RMS
> 0 km	1431289	0.0	5.2	1382108	0.0	2.6
> 10 km	1289873	− 0.1	4.0	1246149	0.0	2.3
> 20 km	1184624	− 0.1	3.3	1144407	0.0	2.1
> 30 km	1091657	− 0.1	3.0	1054542	0.0	2.0
> 40 km	1006212	− 0.1	2.9	971977	0.0	2.0
> 50 km	926797	− 0.1	2.8	895374	0.0	2.0

replacing the NCEI ship-borne from SIO ship-borne. The results are consistent with that V27.1 and DTU13 model are assessed by ship-borne data. Furthermore, with the application of waveform derivative retracking, the accuracy of gravity anomalies has been improved from 6.6 mGal before retracking to 5.5 mGal after retracking over the open ocean, and from 8.9 to 7.4 mGal over the coastal area. The improvement is better than the results obtained by traditional retracking methods (OCOG, 5-β, threshold, Ice-1, and MLE4). It is concluded that the SSH obtained by waveform derivative retracking method is more reliable than of traditional methods. Moreover, the RMS difference between Jason-2/GM-derived and V27.1 is nearly 3.0 mGal, and is 2.0 mGal when replacing the V27.1 from the DTU13. It is indicated that the accuracy of Jason-2/GM-derived is consistent with the V27.1 and DTU13. Therefore, the waveform derivative retracking is an effective method that can be used to improve the quality of SSH, and the accuracy of Jason-2/GM-derived gravity by retracked SSHs is reliable.

Compliance with ethical standards

Conflict of interest The authors declare that they have no conflict of interest.

References

Amarouche L, Thibaut P, Zanife OZ, Dumont JP, Vincent P, Stednou N (2004) Improving the Jason-1 ground retracking to better account for attitude effects. Mar Geod 27(1-2):171–197. https://doi.org/10.1080/01490410490465210

Andersen OB, Knudsen P (1998) Global marine gravity from the ERS-1 and Geosat geodetic mission altimetry. J Geophys Res 103:8129–8137. https://doi.org/10.1029/97jc02198

Andersen OB, Knudsen P, Berry PAM (2010) The DNSC08GRA global marine gravity field from double retracked satellite altimetry. J Geod 84(3):191–199. https://doi.org/10.1007/s00190-009-0355-9

Andersen OB, Knudsen P, Kenyon S, Holmes S (2014) Global and arctic marine gravity field from recent satellite altimetry (DTU13). 76th EAGE Conference and Exhibition. https://doi.org/10.3997/2214-4609.20140897.

Anzenhofer M, Shum CK, Renstch M (1999) Coastal altimetry and applications. Rep.44, Division of Geodetic Science and Surveying. Ohio State University, Columbus

Arabsahebi R, Voosoghi B, Tourian MJ (2018) The inflection-point retracking algorithm: improved Jason-2 sea surface heights in the Strait of Hormuz. Mar Geod 41(4):331–352. https://doi.org/10.1080/01490419.2018.1448029

Bao L, Gao P, Peng H, Jia Y, Shum CK, Lin M, Guo Q (2015) First accuracy assessment of the HY-2A altimeter sea surface height observations: cross-calibration results. Adv Space Res 55(1):90–105. https://doi.org/10.1016/j.asr.2014.09.034

Brown G (1977) The average impulse response of a rough surface and its applications. IEEE J Ocean Eng 2(1):67–74. https://doi.org/10.1109/JOE.1977.1145328

Davis CH (1997) A robust threshold retracking algorithm for measuring ice-sheet surface elevation change from satellite radar altimeters. IEEE T Geosci Remote 35(4):974–979. https://doi.org/10.1109/36.602540

Dumont JP, Rosmorduc V, Picot N, Bronner E, Desai S, Bonekamp H, Figa J, Lillibridge J (2011) OSTM/Jason-2 products hand-book [Online]. https://www.aviso.altimetry.fr/fileadmin/documents/data/tools/hdbk_j2.pdf. Accessed on 2-17-01-13.

Garcia ES, Sandwell DT, Smith WHF (2014) Retracking CryoSat-2, Envisat and Jason-1 radar altimetry waveforms for improved gravity field recovery. Geophys J Int 196(3):1402–1422. https://doi.org/10.1093/gji/ggt469

Gommenginger C, Thibaut P, Fenoglio-Marc L, Quartly G, Deng X, Gómez-Enri J, Challenor F, Gao Y (2011) Retracking altimeter

waveforms near coasts. In: Vignudelli S, Kostianoy AG, Cipollini P, Benveniste J (eds) Coastal altimetry. Springer-Verlag, Berlin Heidelberg, pp 61–102

Guo J, Hwang C, Chang X, Liu Y (2006) Improved threshold retracker for satellite altimeter waveform retracking over coastal sea. Prog Nat Sci 16(7):732–738. https://doi.org/10.1080/10020070612330061

Guo JY, Gao YG, Hwang CW, Sun JL (2010) A multi-subwaveform parametric retracker of the radar satellite altimetric waveform and recovery of gravity anomalies over coastal oceans. Sci China Earth Sci 53(4):610–616. https://doi.org/10.1007/s11430-009-0171-3

Guo J, Shen Y, Zhang K, Liu X, Kong Q, Xie F (2016) Temporal-spatial distribution of oceanic vertical deflections determined by TOPEX/ Poseidon and Jason-1/2 missions. Earth Sci Res J 20(2):H1–H5. https://doi.org/10.15446/esrj.v20n2.54402\

Halimi A, Buller GS, Mclaughlin S, Honeine P (2017) Denoising smooth signals using a Bayesian approach: application to altimetry. IEEE J-STAR 10(4):1278–1289. https://doi.org/10.1109/JSTARS.2016.2629516

Huang Z, Wang H, Luo Z, Shum CK, Tseng KH, Zhong B (2017) Improving Jason-2 sea surface heights within 10 km offshore by retracking decontaminated waveforms. Remote Sens 9(10):1077. https://doi.org/10.3390/rs9101077

Hwang C (1989) High precision gravity anomaly and sea surface height estimation from Geo-3/Seasat altimeter data. Rep. 399, Retrieved from Ohio State University, Columbus.

Hwang C, Parsons B (1995) Gravity anomalies derived from Seasat, Geosat, ERS-1 and TOPEX/POSEIDON altimetry and ship gravity: a case study over the Reykjanes Ridge. Geophys J Int 122(2):551–568. https://doi.org/10.1111/j.1365-246X.1995.tb07013.x

Hwang C, Chang ETY (2014) Seafloor secrets revealed. Sci 346(6205):32–33. https://doi.org/10.1126/science.1260459

Hwang C, Guo J, Deng X, Hsu HY, Liu Y (2006) Coastal gravity anomalies from retracked Geosat/GM altimetry: Improvement, limitation and the role of airborne gravity data. J Geod 80(4):204–216. https://doi.org/10.1007/s00190-006-0052-x

Idris NH, Deng X (2012) The retracking technique on multi-peak and quasi-specular waveforms for Jason-1 and Jason-2 missions near the coast. Mar Geod 35(sup1):217–237. https://doi.org/10.1080/01490419.2012.718679

Idris NH (2019) Regional validation of the Coastal Altimetry Waveform Retracking Expert System (CAWRES) over the largest archipelago in Southeast Asian Seas. Int J Remote Sens 41(15):5680–5694. https://doi.org/10.1080/01431161.2019.1681605

Khaki M, Forootan E, Sharifi MA, Awange J, Kuhn M (2015) Improved gravity anomaly fields from retracked multimission satellite radar altimetry observations over the Persian Gulf and the Caspian Sea. Geophys J Int 202(3):1522–1534. https://doi.org/10.1093/gji/ggv240

Martin TV, Zwally HJ, Brenner AC, Bindschadler RA (1983) Analysis and retracking of continental ice sheet radar altimeter waveforms. J Geophys Res 88(C3):1608–1616. https://doi.org/10.1029/jc088ic03p01608

McCubbine JC, Stagpoole V, Tontini FC, Amos M, Smith E, Winefield R (2017) Gravity anomaly grids for the New Zealand region. New Zeal J Geol Geop 60(4):381–391. https://doi.org/10.1080/00288306.2017.1346692

Ollivier A (2006) Nouvelle approche pour l'extraction de paramtres gophysiques partir des mesures en altimtrie radar, Ph.D. dissertation, Inst. Nat. Polytechnique Grenoble, Grenoble, France.

Passaro M, Cipollini P, Vignudelli S, Quartly GD, Snaith HM (2014) ALES: A multi-mission adaptive subwaveform retracker for coastal and open ocean altimetry. Remote Sens Environ 145:173–189. https://doi.org/10.1016/j.rse.2014.02.008

Pavlis NK, Holmes SA, Kenyon SC, Factor JK (2012) The development and evaluation of the Earth Gravitational Model 2008 (EGM2008). J Geophys Res 117:B04406. https://doi.org/10.1029/2011jb008916

Peng F, Deng X (2017) A new retracking technique for Brown peaky altimetric waveforms. Mar Geod 41(2):99–125. https://doi.org/10.1080/01490419.2017.1381656

Prandi PS, Philipps S, Pignot V, Picot N (2015) SARAL/AltiKa global statistical assessment and cross-calibration with Jason-2. Mar Geod 38(sup1):297–312. https://doi.org/10.1080/01490419.2014.995840

Roscher R, Uebbing B, Kusche J (2017) STAR: Spatio-temporal altimeter waveform retracking via sparse representation and conditional random fields. Remote Sens Environ 201:148–164. https://doi.org/10.1016/j.rse.2017.07.024

Sandwell DT, Garcia E, Soofi K, Wessel P, Smith WHF (2013) Towards 1 mGal global marine gravity from CryoSat-2, Envisat, and Jason-1. Lead Edge 32(8):892–899. https://doi.org/10.1190/tle32080892.1

Sandwell DT, Muller RD, Smith WHF, Garcia E, Francis R (2014) New global marine gravity model from CryoSat-2 and Jason-1 reveals buried tectonic structure. Sci 346(6205):65–67. https://doi.org/10.1126/science.1258213

Shih HC, Hwang C, Barriot JP, Mouyen M, Corréia P, Lequeus D, Sichois L (2015) High-resolution gravity and geoid models in Tahiti obtained from new airborne and land gravity observations: data fusion by spectral combination. Earth Plants Space 67(1):124. https://doi.org/10.1186/s40623-015-0297-9

Shum CK, Ries JC, Tapley BD (1995) The accuracy and applications of satellite altimetry. Geophys J Int 121(2):321–336. https://doi.org/10.1111/j.1365-246X.1995.tb05714.x

Stammer D, Cazenave A (2017) Satellite altimetry over oceans and land surfaces. Taylor & Francis Boca Raton, Florida, p 609

Thibaut P, Poisson J, Ollivier A, Bronner E, Picot N (2009) Singular value decomposition applied on altimeter waveforms. In: Rep. Ocean Surface Topography Sci. Team Meeting, Seattle, WA, USA, June 2009. https://www.aviso.altimetry.fr/fileadmin/documents/OSTST/2009/oral/Thibaut_status.pdf. Accessed Sept 2020

Tseng KH, Shum CK, Yi Y, Emery WJ, Kuo CY, Lee H, Wang H (2013) The improved retrieval of coastal sea surface heights by retracking modified radar altimetry waveforms. IEEE T Geosci Remote 52(2):991–1001. https://doi.org/10.1109/TGRS.2013.2246572

Vignudelli S, Birol F, Benveniste J, Fu LL, Picot N, Raynal M, Ronard H (2019) Satellite altimetry measurements of sea level in the coastal zone. Surv Geophys 40(6):1319–1349. https://doi.org/10.1007/s10712-019-09569-1

Wang J, Guo J, Liu X, Shen Y, Kong Q (2018) Local oceanic vertical deflection determination with gravity data along a profile. Mar Geod 41(1):24–43. https://doi.org/10.1080/01490419.2017.1380091

Wessel P, Watts AB (1988) On the accuracy of marine gravity measurements. J Geophys Res 93(B1):393–413. https://doi.org/10.1029/JB093iB01p00393

Wessel P, Smith WHF, Scharroo R, Luis J, Wobbe F (2013) Generic mapping tools: improved version released. EOS Trans Am Geophys Union 94(45):409–410. Wingham. https://doi.org/10.1002/2013eo450001

Wingham D J, Rapley CG, Griffiths H (1986) New techniques in satellite altimeter tracking systems. in Proceedings of the IGARSS'86 Symposium, Zurich, Switzerland, September.

Xu XY, Birol F, Cazenave A (2018) Evaluation of coastal sea level offshore Hong Kong from Jason-2 altimetry. Remote Sens 10(2):282. https://doi.org/10.3390/rs10020282

Yang Y, Hwang C, Hsu HJ, Dongchen E, Wang H (2012) A subwaveform threshold retracker for ERS-1 altimetry: a case study in the Antarctic Ocean. Comput Geosci 41:88–98. https://doi.org/10.1016/j.cageo.2011.08.017

Yuan J, Guo J, Liu X, Zhu C, Niu Y, Li Z, Ji B, Ouyang Y (2020a) Mean sea surface model over China seas and its adjacent ocean established with the 19-year moving average method from multi-satellite altimeter data. Cont Shelf Res 192:104009. https://doi.org/10.1016/j.csr.2019.104009

Yuan J, Guo J, Niu Y, Zhu C, Li Z, Liu X (2020b) Denoising effect of Jason-1 altimeter waveforms with singular spectrum analysis: a case study of modelling mean sea surface height over South China Sea. J Mar Sci Eng 8(6):426. https://doi.org/10.3390/jmse8060426

Zhang S, Sandwell DT, Jin T, Li D (2017) Inversion of marine gravity anomalies over southeastern China seas from multi-satellite altimeter vertical deflections. J Appl Geophys 137:128–137. https://doi.org/10.1016/j.jappgeo.2016.12.014

Zhang S, Li J, Jin T, Che D (2018) HY-2A altimeter data initial assessment and corresponding two-pass waveform retracker. Remote Sens 10(4):507. https://doi.org/10.3390/rs10040507

Zhu C, Guo J, Hwang C, Gao J, Yuan J, Liu X (2019) How HY-2A/GM altimeter performs in marine gravity derivation: assessment in the South China Sea. Geophys J Int 219:1056–1064. https://doi.org/10.1093/gji/ggz330

Zhu C, Guo J, Gao J, Liu X, Hwang C, Yu S, Yuan J, Ji B, Guan B (2020) Marine gravity determined from multi-satellite-GM/ERM altimeter data over the South China Sea: SCSGA V1.0. J Geod 94(5):50. https://doi.org/10.1007/s00190-020-01378-4